Experimental test on the applicability of the standard retardation condition to bound magnetic fields

A. L. Kholmetskii
Faculty of Physics, Belarus State University, Nezavisimosti Avenue 4, 220080, Minsk, Belarus

O. V. Missevitch
Institute for Nuclear Problems, Bobruiskaya 11, 220050, Minsk, Belarus

R. Smirnov-Rueda[a)]
Applied Mathematics Department, Faculty of Mathematics, Complutense University, 28040 Madrid, Spain

R. Ivanov and A. E. Chubykalo
Faculty of Physics, University of Zacatecas, C-580, Zacatecas 98068, ZAC., Mexico

(Received 13 July 2006; accepted 6 November 2006; published online 31 January 2007)

We start with the fact that the actual consensus on the empirical verification of the standard retardation condition does not take into account the complex structure of the whole electromagnetic field in the near zone. The most rigorous and methodologically consistent way to the empirical test of the causal behavior of the whole EM field should be based on testing causal properties for each component—velocity dependent (bound) and acceleration dependent (radiation)—taken separately. Preliminary discussions on the relative contribution of bound and radiation terms for an idealized magnetic dipole provided us with a methodological approach to causal characteristics of bound fields. In view of practical implementation of this method, we made an analysis of the finite size loop antennas. The use of multisection loop antennas was fully justified by a substantial rise of the ratio of bound-to-radiation field strength. Finally, we effected numerical calculations, taking into account particular experimental settings. Comparison with the experimentally obtained data showed considerable discrepancy with the predictions of the standard electromagnetic theory. A possible interpretation in terms of nonlocal properties of bound fields in near zone is proposed. © *2007 American Institute of Physics*. [DOI: 10.1063/1.2409771]

I. INTRODUCTION

The current causal status of the modern classical electromagnetic (EM) field theory is primarily associated with the empirical fact of fundamental importance: Hertz's generation of EM waves according to Maxwell's theory. In maintaining the actual consensus on the definitive empirical verification of the retardation effects taking place for the EM field, the underlying fundamental structure of the whole field in the near zone should not be underestimated, i.e., the fact that it is composed from bound and radiation components, essentially different by nature. Therefore, the most rigorous and methodologically consistent approach to the empirical test of the causal behavior of the whole EM field consists in testing causal properties for each component taken separately. The common scientific literature shows that no one intention of this kind has been made since the time of Hertz's experiments. As a consequence, we propose in this work methodologically new insight on the empirical verification of the type of causal (retardation) conditions for radiation and bound field components.

The most general approach to the calculation of electric and magnetic fields is explicable in terms of the standard expression for field strengths of an arbitrary moving point charge[1,2]

$$\mathbf{E}=\frac{q}{(4\pi\varepsilon_0)}\left\{\left[\frac{(\mathbf{n}-\mathbf{u}/c)(1-(\mathbf{u}/c)^2)}{(1-(\mathbf{n}\cdot\mathbf{u})/c)^3R^2}\right]_c+\left[\frac{\mathbf{n}}{(1-(\mathbf{n}\cdot\mathbf{u})/c)^3R}\times\left\{\left(\mathbf{n}-\frac{\mathbf{u}}{c}\right)\times\frac{\dot{\mathbf{u}}}{c}\right\}\right]_c\right\}, \quad (1)$$

$$\mathbf{B}=[\mathbf{n}\times\mathbf{E}], \quad (2)$$

where the corresponding quantity in brackets means that it is evaluated at the retarded time $t'=t-R/c$; R is the distance from the retarded position of the charge to the point of observation and $\mathbf{u}$ is a velocity of a charge at the instant of time t'; $\mathbf{n}=\mathbf{R}/R$.

Both electric $\mathbf{E}$ and magnetic $\mathbf{B}$ fields are composed of two essentially different parts

$$\mathbf{E}=\mathbf{E_u}+\mathbf{E_a};\quad \mathbf{B}=\mathbf{B_u}+\mathbf{B_a}, \quad (3)$$

where $\mathbf{B_u}=\mathbf{n}\times\mathbf{E_u}$ and $\mathbf{B_a}=\mathbf{n}\times\mathbf{E_a}$.

The first terms $\mathbf{E_u}$ and $\mathbf{B_u}$ are usually regarded as velocity fields because they are independent of acceleration $\dot{\mathbf{u}}$. The electric velocity field $\mathbf{E_u}$ falls off as R^{-2} that is the substantial feature of the radial (longitudinal) field components associated with the static Coulomb law. By this reason the velocity fields are also referred as bound fields. On the contrary, the second part of solutions (1) and (2), denoted as $\mathbf{E_a}$ and $\mathbf{B_a}$ are linear functions of acceleration, falling off proportional to R^{-1}. These terms are responsible for the radiation and take

a)Electronic mail: smirnov@mat.ucm.es

no place in the case of uniformly moving charge (as well as at rest), giving priority to bound components in the formation of EM field.

The latter fact poses a basic question concerning the nature and physical characteristics on bound fields: it implies a fundamental uncertainty of whether the applicability of the standard retardation condition to all components of the electromagnetic field has solid methodological and empirical grounds. Does the conventional experimental approach take into account the complex structure of the whole field and should there be an explicit empirical test of the applicability of the retardation (causal) condition to bound and radiation field components each taken separately?

The peculiar historical background of the classical EM theory gives an additional motivation to focus our attention on such a question. The problem of propagation of EM interactions was the crucial point in choosing appropriate theoretical foundations for classical electrodynamics in the 19th century. By the time Hertz began his experiments in providing evidence in favor of EM waves traveling in air with the velocity of light (i.e., in favor of the standard retardation condition), the set of fundamental solutions to Maxwell's equations did not imply any explicit separation into bound and radiation field components. Only Lorentz's modification of Maxwell's theory (1892) provided Lienard (1898) and Wiechert (1901) with inhomogeneous wave equations. The retarded solutions were found under the retardation constraint which, as it is generally perceived, was just experimentally verified by Hertz in 1888 (Ref. 3) for the whole EM field. It gave rise to the acceptance of a fundamental viewpoint on the bound and radiation field components of the Lienard-Wiechert theoretical solutions having the same rate of propagation (or retardation).

Thus, in light of our discussion we can see that Hertz's experiments were not especially thought-out in testing the applicability of the retardation constraint on different components of the whole EM field. On the contrary, the main Hertz's effort was directed in establishing the reality of EM waves traveling in air as Maxwell's theory predicted. Since the time of Hertz's experiments no one has claimed the need of testing explicitly the applicability of the standard retardation condition to the bound fields. Nevertheless, this separate test should have been suggested as soon as the Lienard-Wiechert structure of the whole EM field became generally recognized as corresponding to the physical reality. Moreover, this attitude should have been recommended and justified on a methodological basis since the intensity of bound fields fall off much faster than the strength of radiation components and, therefore, bound fields become negligible already at very short distances (i.e., outside the near zone).

In addition to the feebleness of the effects produces by bound fields, there is also one technical circumstance that made any direct experimental approach to causal characteristics of bound fields an extremely difficult task. In fact, all known radiation devices (antennas, etc.) are designed to enhance the radiation to the utmost, i.e., to reach the maximum value of the ratio of radiation-to-bound field strength. In other words, the use of radiation devices in their traditional form is rather counterproductive and there should be a radically different experimental approach based on an additional technical effort in producing a substantial rise of the ratio of bound-to-radiation field strength, i.e., capable to stand out the contribution of bound components to the detriment of EM radiation.

As follows, we shall present an experimental scheme that is methodologically conceived to surmount all of the abovementioned technical difficulties and to provide unambiguous explicit information on bound magnetic components. The main idea of our method is based on the analysis of the EM field in the plane of the loop antenna with an oscillating current. Section II is devoted to the underlying idea of how the empirical test of the retardation conditions can be conceived in an idealized case. In Sec. III a methodological approach will be described in greater detail as it concerns a particular experimental setup (described in Sec. IV), which implements a multisection type of antenna in order to increase the ratio of bound-to-radiation field strength. Finally, Sec. V presents results of numerical calculations and their comparison with experimental data.

II. THE STRUCTURE OF EM FIELD DUE TO AN IDEALIZED MAGNETIC DIPOLE

A. Introduction into methodology of experimental approach

By analogy with the retarded vector potential $\mathbf{A}$, the magnetic field $\mathbf{B}$ can be determined directly by the standard expression[4,5]

$$\mathbf{B}(R,t)=\frac{1}{4\pi\varepsilon_0 c^2}\int\left[\frac{\nabla_s\times\mathbf{J}(r_s)}{R}\right]_c dV_s \tag{4}$$

as the retarded solution of the corresponding D'Alembert equation

$$\Delta\mathbf{B}-\varepsilon_0\mu_0\frac{\partial^2\mathbf{B}}{\partial t^2}=-\mu_0\nabla\times\mathbf{J}, \tag{5}$$

where $\mathbf{J}$ is the conduction current density; $\mathbf{B}=\nabla\times\mathbf{A}$ and the quantity placed inside the square bracket in Eq. (4) is measured at the retarded time $t'=t-R/c$.

In the low velocity relativistic limit[4,5] (i.e., when the velocity of charges is much lower than c but the effect of retardation is still taken into account) for filamentary closed circuit, the general solution (4) can be presented in an equivalent form of the line integral[4]

$$\mathbf{B}=\mathbf{B_u}+\mathbf{B_a}=\frac{1}{4\pi\varepsilon_0 c^2}\oint_\Gamma\left\{\frac{[I]_c}{R^2}+\frac{[\dot{I}]_c}{cR}\right\}\mathbf{k}\times\mathbf{n}dl, \tag{6}$$

where $\mathbf{n}=\mathbf{R}/R$; I is the conduction current; $\mathbf{k}$ is the unit vector in the direction of $\mathbf{I}$, i.e., $\mathbf{I}=I\mathbf{k}$, and dl is an infinitesimal element of the loop line Γ.

Equation (6) is exact when the centripetal acceleration of the moving charges is ignored at a low velocity approximation and, as it is demonstrated in Ref. 5 can be derived directly, starting with the D'Alembert equations for retarded potentials φ and $\mathbf{A}$. As a consequence, Eq. (6) has a general applicability to usual electric circuits since the velocity of conduction electrons is always much lower than c. The first

term on the right-hand side of expression (6) is the classical integral form of the Biot-Savart law when the current I in the circuit Γ is steady (i.e., $\dot{I}=0$).

The velocity dependent (bound) component $\mathbf{B_u}$ arises from the term proportional to $[I]_c$ whereas the acceleration field $\mathbf{B_a}$ is due to the $[\dot{I}]_c$ term. Traditionally, in the general (time-dependent) case solutions to corresponding D'Alembert equations are found under the retardation constraint applied to the whole EM field, i.e., providing the same retardation rates to bound and radiation fields as it takes place in the standard Eq. (6). In view of overwhelming empirical evidences that radiation components propagate at the velocity of light c, one should follow the actual consensus and keep the standard retardation constraint unmodified in respect to acceleration fields $\mathbf{B_a}$.

Since the general proposal of this work is to elaborate a consistent methodological scheme in order to empirically test the type of causal behavior meaningful for bound fields, we take the retardation condition in respect to bound fields as unknown and allow all possible values for the retardation parameter v, i.e., the situation when the retardation effects attached to the propagation velocity of bound fields $\mathbf{B_u}$, denoted as v, can take any value from the range $v>0$. In context of this methodological approach, with no special preference for any particular value of the retardation parameter v (for instance, $v=c$), we have

$$\mathbf{B}=\mathbf{B_u}+\mathbf{B_a}=\frac{1}{4\pi\varepsilon_0 c^2}\int\left\{\frac{[I]_v}{R^2}+\frac{[\dot{I}]_c}{cR}\right\}\mathbf{k}\times\mathbf{n}dl, \qquad (7)$$

where the quantity in square bracket $[I]_v$ means that it is evaluated at the different retarded time $t'_v=t-R/v$.

There is no need for any theoretical justification of Eq. (7) because it makes sense only as a tool for testing the validity of the standard retardation condition $v=c$. In other words, Eq. (7) is taken to make reliable theoretical predictions only for $v=c$ as the standard theory requires. In this case if there are some observable discrepancies between the experimental observations and theoretical predictions based on $v=c$, Eq. (7) can be taken as a first approximation to make empirical estimation of the type of retardation condition required for bound field components.

For further convenience, let us resort to a certain idealization in our attempt to use the basic Eq. (7) in a less cumbersome representation, keeping all the fundamental features related to the bound and radiation components untouched. For these reasons, we first consider an example of idealized oscillating magnetic dipole given in form of a loop antenna with the radius r. The idealization implies two requirements: (a) The radius of the loop r is considerably smaller than the distance R from the center of the antenna to the point of observation; (b) the wavelength λ of emitted EM radiation greatly exceeds the perimeter of the loop, i.e., $r\ll\lambda$. The second requirement (b) means that a magnitude of the conduction current I has nearly the same value in all parts of the loop circuit at a present instant of time t. This condition is usually regarded as an approximation of quasi-stationary current.

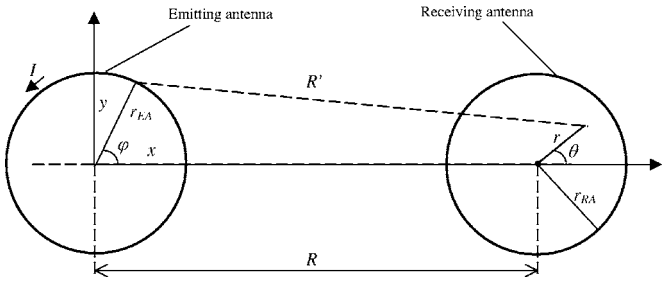

FIG. 1. The "in-plane configuration:" The emitting and receiving antenna loops belong to the same plane.

Having assumed the above idealizations, the results of Eq. (7) are considerably simplified. By analogy with the standard procedure[5] implemented for $v=c$, all contributions into the magnetic field in the plane of an oscillating magnetic dipole for any particular value v from the range $0<v<\infty$ are

$$\mathbf{B}(R,t)=-\frac{\Delta S}{4\pi\varepsilon_0 c^2}\left\{\frac{[I]_v}{R^3}+\frac{c}{v}\frac{[\dot{I}]_v}{cR^2}+\frac{[\ddot{I}]_c}{c^2R}\right\}\mathbf{z}, \qquad (8)$$

where ΔS is the area bounded by the loop of emitting antenna (a reader interested in the full derivation of (8) can refer to the Appendix).

If $v=c$, Eq. (8) takes the standard form obtained in the low velocity relativistic limit[5,6]

$$\mathbf{B}(R,t)=-\frac{\Delta S}{4\pi\varepsilon_0 c^2}\left\{\frac{[I]_c}{R^3}+\frac{[\dot{I}]_c}{cR^2}+\frac{[\ddot{I}]_c}{c^2R}\right\}\mathbf{z}. \qquad (9)$$

The first and the second terms in the right-hand side (rhs) of Eq. (8) have the common origin and arise from the bound component $\mathbf{B_u}$. The contribution proportional to R^{-3} is a dynamic counterpart of a steady magnetic field produced by a static magnetic dipole. The R^{-2}-term is due to a finite size of the antenna loop which stipulates the difference in the value of retarded time $t'=t-R/c$ for EM signals out-coming from different segments of the perimeter of EA. In other words, a bound field perturbation emitted from the nearest half of the loop arrives at the point of observation before an equivalent signal from the farthest half. This retarded time shift leads to the contribution proportional to $\dot{I}$ (for a more detailed explanation, see the Appendix). The last term corresponds to the magnetic dipole radiation which falls off as R^{-1}.

Let us now take into consideration a receiving loop antenna (RA) under the set of approximations assumed earlier for the emitting antenna (EA). Let us place both EA and RA loops in the same plane xy as it is shown in Fig. 1. The origin of the coordinate frame coincides with the center of the EA loop and R is the distance between the centers of EA and EA. The generation of an electromotive force (EMF) $\varepsilon(t)$ is proportional to the time variation of the magnetic field flux (which is an empirically established integral form of the Faraday law)

$$\varepsilon(t)=-\frac{d}{dt}\iint_S \mathbf{B}\cdot\mathbf{z}dS. \qquad (10)$$

The time variation of the magnetic field $\mathbf{B}(t)$ in the area of the RA is determined by the change of the conduction cur-

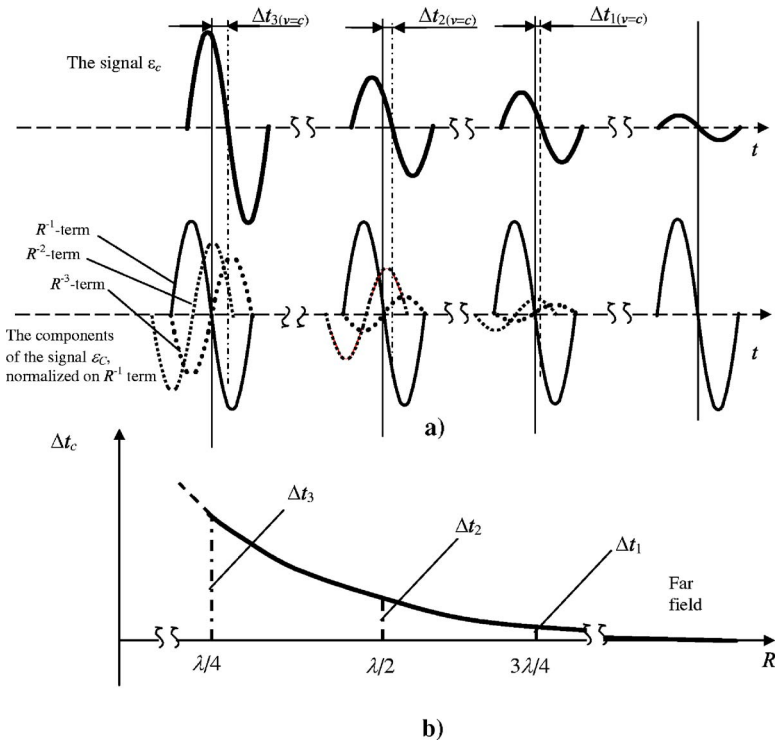

FIG. 2. (a) Relative positions of R^{-3}, R^{-2}, R^{-1} components and their superposition at distances $R=\lambda/4$, $\lambda/2$, $3\lambda/4$, and $R\gg\lambda$. (b) $\Delta t(R)$-dependence represents the time shift Δt between zero-crossing points of the whole and reference signals as a function of a distance R under the standard retardation condition $v=c$.

rent $I(t)$ in the circuit of the EA. If the area $\Delta S=\pi r_{\mathrm{EA}}^2$ bounded by the loop of the EA equals that of the RA (i.e., $r_{\mathrm{EA}}=r_{\mathrm{RA}}$), then in the approximation of the quasi-stationary current the wavelength λ of the EM radiation also greatly exceeds the radius r_{RA} of the RA. In other words, the magnetic field **B** has nearly the same strength in all parts of the surface S bounded by the loop of the RA, so that

$$\varepsilon(t)=-\frac{dB}{dt}\iint_S dS=\frac{(\Delta S)^2}{4\pi\varepsilon_0 c^2}\left\{\frac{[\dot{I}]_v}{R^3}+\frac{c}{v}\frac{[\ddot{I}]_v}{cR^2}+\frac{[\dddot{I}]_c}{c^2R}\right\}, \quad (11)$$

where $B=\mathbf{B}\cdot\mathbf{z}$ is the component of the magnetic field in **z**-direction.

At $v=c$ we get from (11) the standard expression for the EMF $\varepsilon(t)$. However, the second R^{-2}-term disappears in the strong limit $v=\infty$. This case implies no retardation effects for bound fields and at the point of observation every perturbation emitted from the nearest half part of the loop will be counteracted by an equivalent signal from the farthest half part. Therefore, the in-plane geometry shown in Fig. 1 should be sensitive to any variation of the retardation parameter v, since it directly affects the value of the second R^{-2}-term.

B. Idealized harmonic signal's approximation

Let us first assume for simplicity that current I in the EA oscillates harmonically at angular frequency ω as $I(t)=I(0)\cos(\omega t)$.

1. Standard retardation condition

In approximation of the harmonic conduction current and considering the standard retardation condition $v=c$ with respect to bound fields, Eq. (11) yields

$$\varepsilon_c(t)=\varepsilon(0)\left[-\frac{\sin\omega(t-R/c)}{R^3}-\frac{\omega\cos\omega(t-R/c)}{cR^2}+\frac{\omega^2\sin\omega(t-R/c)}{c^2R}\right], \quad (12)$$

where $\varepsilon_c(0)=[(\Delta S)^2 I(0)\omega]/4\pi\varepsilon_0 c^2$ and $-\omega(R/c)$ is the phase shift due to retardation effects.

Contributions into the induced EMF $\varepsilon_c(t)$ are functions of ω, t, and R. At large distances the radiation R^{-1}-term predominates and it can be taken as a reference signal $\varepsilon_r(t)$

$$\varepsilon_r(t)=\frac{\varepsilon_r(0)}{R}\sin\omega\left(t-\frac{R}{c}\right). \quad (13)$$

It is convenient to specify in Eq. (12) relative phase shifts of R^{-3}, R^{-2} contributions and R^{-1}-term which is in phase with the reference signal (13)

$$\varepsilon_c(t)=\varepsilon(0)\left[\frac{\sin(\omega(t-R/c)-\pi)}{R^3}+\frac{\omega\sin(\omega(t-R/c)-\pi/2)}{cR^2}+\frac{\omega^2\sin\omega(t-R/c)}{c^2R}\right]. \quad (14)$$

It follows from Eq. (14) that corresponding phases of R^{-3} and R^{-2}-terms drop behind the phase of the reference signal at $-\pi$ and $-\pi/2$, respectively. In other words, R^{-3} and R^{-2} contributions need additional times π/ω and $\pi/2\omega$ to come up with the phase $\omega(t-R/c)$ of the reference signal measured at an instant of time t, as we specified in Fig. 2(a).

At very short distances the R^{-3}-term makes a dominant contribution so that the phase of the resultant signal $\varepsilon_c(t)$ acquires a difference $-\pi$ in comparison with the phase of the

reference signal $\varepsilon_r(t)$. As R gets larger, R^{-2} and R^{-1} terms provide more considerable contribution. At relatively large distances when R^{-1}-term already predominates, the phase of $\varepsilon_c(t)$ tends to the phase of the reference signal $\varepsilon_r(t)$. It explains why at relatively small distances (when R^{-3}-term still makes notable contribution) there is always a finite time shift Δt between instants when both signals $\varepsilon_c(t)$ and $\varepsilon_r(t)$ cross a zero line. To illustrate the role of retardation effects in giving a resultant $\varepsilon_c(t)$ as it stands from Eq. (14), we show in Fig. 2(a) examples of relative positions of $\varepsilon_c(t)$ and $\varepsilon_r(t)$ at some fixed R. Continuous vertical line at different moments of time shows a zero-crossing point for the reference R^{-1}-signal at $R=\lambda/4$, $\lambda/2$, $3\lambda/4$, and $R\gg\lambda$ (far field). Dot vertical line corresponds to a zero-crossing point for the resultant signal $\varepsilon_c(t)$The distance on the time axis t between both vertical lines we denote as Δt.

Thus, as it follows from Eq. (14), the time shift Δt reaches the maximum value $\Delta t=\pi/\omega$ as $R\to 0$ and tends to $\Delta t=0$ as $R\to\infty$. Starting with Eq. (14) we calculated the value of Δt as a function of R and plotted it in Fig. 2(a). The reduction of Δt shows considerable descending rates in the very near zone $R\leq\lambda/4$ in comparison with moderate rates within $\lambda/4\leq R\leq\lambda$ and it tends to vanish at far zone $R\gg\lambda$. In other words, R^{-2} and R^{-3}-contributions into the whole signal $\varepsilon_c(t)$ are responsible for a positive time shift Δt in comparison with the instant of time when R^{-1} reference signal crosses a zero line.

The $\Delta t(R)$-dependence presented at Fig. 2(a) is worth commenting from the following viewpoint. Since all R^{-3}, R^{-2}, and R^{-1} contributions into the resultant EMF $\varepsilon_c(t)$ propagate at the light velocity c as it does the reference signal $\varepsilon_r(t)$, hence the reduction of the time shift Δt means that at relatively small distances $(0\leq R\lesssim\lambda)$ the zero-crossing point of the resultant signal propagates faster than the zero-crossing point of the reference signal, i.e., faster than the velocity of light. It is clear that it is only apparent superluminality since each component of the whole signal does not succeed the velocity of light.

2. General retardation condition with respect to bound fields

Let us now consider a wide range of variation $0<v<\infty$ for the retardation parameter v with respect to bound fields. First we note that the quasi-stationary current approximation $r\ll\lambda$ (or $r/c\ll 2\pi/\omega$) remains valid for bound components in the range $v\geq c$, i.e., $r/v\ll 2\pi/\omega$. Contrarily, the condition $r/v\ll 2\pi/\omega$ cannot be sustained for all possible values of the retardation parameter from $0<v\leq c$ because there should be the lowest (critical) value v_{cr} and, therefore, for values $v<v_{cr}$ the quasi-stationary current approximation will not already be viable.

Thus, considering some value v from $v_{cr}<v<\infty$ compatible with the quasi-stationary current approximation, Eq. (11) gives

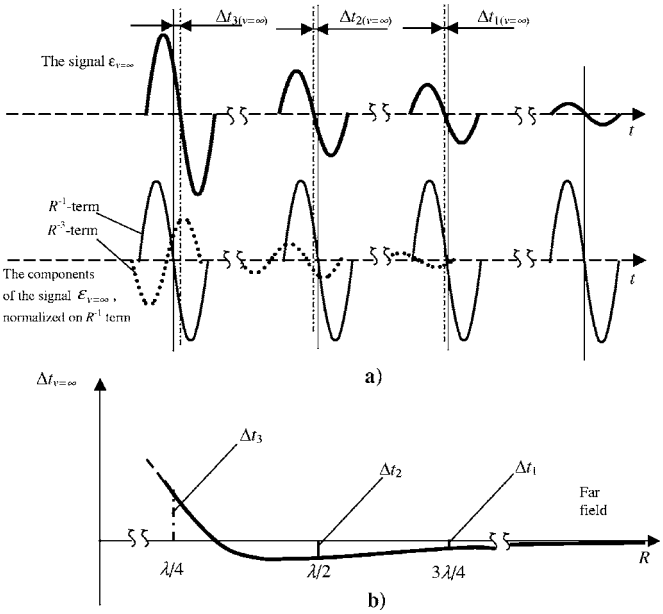

FIG. 3. (a) Relative positions of R^{-3}, R^{-1} components and their superposition at distances $R=\lambda/4$, $\lambda/2$, $3\lambda/4$, and $R\gg\lambda$. (b) $\Delta t(R)$-dependence represents the time shift Δt between zero-crossing points of the whole and reference signals as a function of a distance R under the retardation condition $v=\infty$.

$$\varepsilon_v(t)=\varepsilon(0)\left[\frac{\omega-(t-R/v)-\pi}{R^3}+\frac{\omega\sin(\omega-R/\nu)-\pi/2}{vR^2}+\frac{\omega^2\sin\omega(t-R/c)}{c^2R}\right], \tag{15}$$

where $-\omega R/\nu$ and $-\omega(R/c)$ are respective phase shifts due to retardation effects of bound and radiation fields.

To illustrate the difference with Eq. (14) we consider a strong limit $v=\infty$ when R^{-2}-term disappears and only R^{-3} and R^{-1}-terms remain as it is shown in Fig. 3(a). There is a novel feature in comparison with the standard case $v=c$: the time shift $\Delta t_{v=\infty}$ reaches negative values for $R\gtrsim\lambda/2$. Starting with Eq. (15) we calculated the value of $\Delta t_{v=\infty}$ as a function of R and plotted it in Fig. 3(b).

The above-considered analysis used for the standard condition $v=c$ and a strong limit $v=\infty$ is equally applicable in general case and can be implemented for any value v from $v_{cr}<v<\infty$. One can obtain numerically from Eq. (15) that for the range $c<v<\infty$, all $\Delta t(R)$-dependencies exhibit negative minimum and higher descending rates of $\Delta t(R)$ than the curve for $v=c$. On the contrary, for $v<c$ all $\Delta t(R)$ have lower descending rates approximately within $R\lesssim\lambda/4$.

We have thus reached a conclusion that the type of variation of $\Delta t(R)$ is sensitive to a particular value of the retardation parameter v. More specifically, the standard condition $v=c$ with respect to bound fields does not imply any negative Δt values and hence this prediction of the standard EM theory can be subjected to the empirical test. Further on we shall refer to this approach as the zero-crossing method.

C. Realistic pulsed mode approximation

Perturbations produced by reflected EM waves (experimental data are measured in a closed laboratory room) make

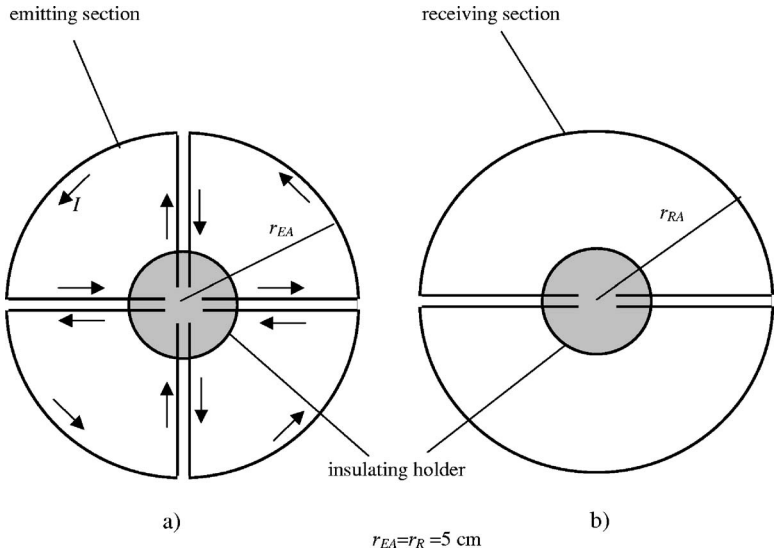

FIG. 4. (a) The emitting antenna (EA) cross section (the arrows show the current direction in all subsections). (b) The receiving antenna (RA) cross section.

unviable any practical implementations of the above-considered idealized approach based on the generation of a continuous harmonic signal. As a consequence, one has to undertake all experiments in such a manner that during the observations, no perturbation received by the RA could be associated with the reflected radiation. It can be achieved if the practical realization is based on the excitation of one very short quasi-harmonic signal.[7] Nowadays, such pulsed mode generation is used in the standard EM-radiation metrology techniques in order to avoid interference with reflected waves.

Further on we shall assume that at $t<0$ there is no voltage applied on the EA, i.e., $U=0$, and $U=U(t)$ has nonzero magnitude at $t\geq 0$. If $U(t)$ is known as a function of time t explicitly, then the shape of the emitted signal can be found directly from Kirchhoff's equation written for the emitting circuit as

$$U_L + U_{R_e} + U_C = U(t), \tag{16}$$

where R_e is the characteristic resistance of the EA.

Taking into account standard relationships such as $U_L = L(dI/dt) = L(d^2Q/dt^2)$, $U_C = Q/C$ (where Q denotes the charge), and neglecting the resistance R_e (this approximation is valid when forced oscillations take place), Eq. (16) obtains the form

$$\frac{d^2Q}{dt^2} + \omega_0^2 Q = \omega_0^2 U(t), \tag{17}$$

where $\omega_0 = 1/\sqrt{LC}$ is the proper frequency of the emitting circuit.

We assume that the voltage $U(t)$ applied to the spark gap circuit, reaches its maximum value at $t=0$ and after the discharge through the spark gap $U(t)$ exponentially falls down to zero. If the characteristic time τ of exponential decay $U(t)\sim U(0)\exp(-t/\tau)$ is less (or comparable) with ω_0^{-1}, then based on Eq. (17), one can treat the generated charge $Q(t)$ and current $I(t)=dQ(t)/dt$ as quasi-harmonic functions for $t\geq 0$, and as zero constants at $t<0$. This approximation will be achieved in our experimental realization, keeping $\Delta t(R)$-dependencies (recalculated for realistic pulsed mode approximation) equally sensitive to a particular value of the retardation parameter v.

III. METHODOLOGY OF EXPERIMENT IN THE CASE OF MULTISECTION ANTENNAS

In this section we discuss the methodology of experimental approach to bound fields in the case of multisection EA and RA that constitute a practical realization of particular experimental scheme considered in Sec. IV. The requirements imposed by the quasi-stationary current approximation are hardly available in real experimental practice. On the one hand, the value of the EMF ε depends essentially on the radius r of the loop antenna because it is proportional to $(\Delta S)^2 \sim r^4$. On the other hand, in order to reach the criteria of the quasi-stationary current approximation, one cannot decrease the radius r without moderation, since the precision of measurements critically depends on the intensity of EA and RA signals. Therefore, there should be a balance between mutually excluding requirements. In our attempt to reduce dependence on the radius of the loop r, we resorted to the help of so-called multisection antennas. The approximation of the quasi-stationary current and the maximum ratio of bound-to-radiation field strength can be easily implemented for finite size multisection antennas (even in the range of high frequencies ω), keeping valid the approach based on the zero-crossing method.

The EA and RA are composed from four and two sections, respectively, as it is shown in Fig. 4. The arrows mean directions of conduction currents at some given instant of time. Therefore, the symmetric form of multisection EA and RA implies no net current in radial directions. In fact, all radial parts of each section make no contribution in generation of magnetic fields (bound or radiation) due to the cancellation of current flows in adjacent parts of neighbor sections. This property is important to reduce considerably undesirable electric dipole radiation in the case of EA and, in addition, to suppress any disturbing effect produced by electric dipole radiation in RA.

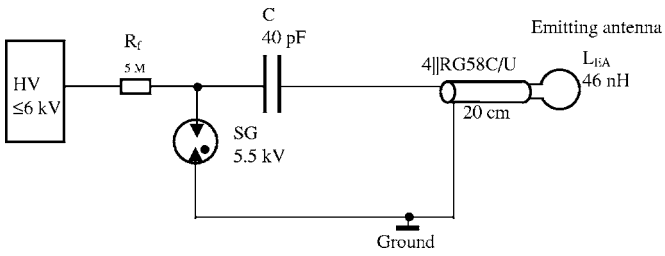

FIG. 5. Technical realization of EA driving circuit.

Since the conduction current is delivered to four sections of the EA simultaneously, the resultant magnetic field is determined entirely as a superposition of magnetic fields created by each section. Therefore, the applicability of the approximation of the quasi-stationary current resides on its validity for every independent section. As a consequence, we can consider the criteria for the quasi-stationary current approximation of a multisection antenna as

$$\omega \ll \omega_c = \frac{2\pi nc}{r}, \tag{18}$$

where ω_c denotes the critical value of the frequency of oscillations and n means the number of sections.

To generate pulsed mode EM signals, we used short quasi-sinusoidal current bursts feeding of the EA. As we already mentioned in Sec. II C, such pulsed EM signals are used to avoid interference with reflected waves during experimental observations. Moreover, pulsed mode excitation procedure allowed us to reduce the average power to the realistic level available in the majority of physics laboratories. In order to get reliable experimental data (at a distance $\sim$3 m) under the continuous mode generation, one will need the high peak power of $\sim$10 kW which is rather unrealistic.

Let us now describe a technical realization of the experimental setup in regards to the emitting multisection antenna (see Fig. 5). A fast high-voltage spark gap (SG) constitutes the driving circuit of the EA and it is connected with the multisection emitting circuit via the blocking capacitor C which also plays the role of the energy storage element. Nowadays, the spark gap excitation circuit remains among the best generators of fast ($\sim$1 ns) high-voltage (5 kV) pulses with high current capability ($\sim$1 kA). The whole circuit, presented in Fig. 5, can be viewed as LC-contour with the resonance frequency $\omega_0 = 1/\sqrt{LC}$, where L is the inductance of the EA.

The high-voltage supply (HV) is connected to the EA via the resistor R_f. The latter determines the time necessary to charge the capacitor C as well as the duration of the period in a series involving successive charges and discharges. We also assume that values of L, C, and the radius r, are given in the range of applicability of the approximation of the quasi-stationary current, i.e., $\omega_0 \ll \omega_c$.

We consider the case when both loops of the EA and RA belong to the same plane xy (see Fig. 1). Therefore, Eq. (7) provides us with the resultant magnetic field **B** produced by the EA

$$\mathbf{B} = \frac{1}{4\pi\varepsilon_0 c^2} \oint_\Gamma \left\{ \frac{[I]_v}{R'^2} + \frac{[\dot{I}]_c}{cR'} \right\} d\mathbf{l} \times \mathbf{n}_{R'}, \tag{19}$$

where $R'_x = R + r\cos\theta - r_{\mathrm{EA}}\cos\varphi$, $R'_y = r\sin\theta - r_{\mathrm{EA}}\sin\varphi$, $R'_z = 0$, $d\mathbf{l}$ is an infinitesimal element of the emitting loop Γ, and $\mathbf{n}_{R'} = \mathbf{R}'/R'$ is the unit vector.

EMF $\varepsilon(t)$ induced in the RA can be calculated according to the integral form of the Faraday induction law

$$\varepsilon = -\frac{d}{dt}\int_{S_{\mathrm{RA}}} \mathbf{B}(R,t)\cdot d\mathbf{S} = -\int_0^{2\pi}\int_0^{r_{\mathrm{RA}}} \frac{dB_z(R,t)}{dt} r dr d\theta, \tag{20}$$

where S_{RA} and r_{RA} are the area and the radius of the RA, respectively, as it is shown in Fig. 1.

We are now in a position to approach realistic numerical evaluation of the output signal in the RA, starting with Eqs. (19) and (20). Since we assume valid the approximation of quasi-stationary current, i.e., $\omega \ll \omega_c$, then at a given instant of time t the conduction current has nearly the same magnitude I in all parts of the loop of the EA. Having this approximation in mind, we obtain

$$\varepsilon_p = \frac{1}{4\pi\varepsilon_0 c^2}\int_0^{r_{\mathrm{RA}}}\int_0^{2\pi}\int_0^{2\pi}\left[\frac{[\dot{I}]_v}{R'^3} + \frac{[\ddot{I}]_c}{R'^2}\right]\Omega(R,r,\theta,\phi) r_{\mathrm{EA}}^2 r dr d\theta d\varphi, \tag{21}$$

where $\Omega(R,r,\theta,\varphi) = 1 - r/r_{\mathrm{EA}}\cos(\theta-\varphi) - r/r_{\mathrm{EA}}\cos\varphi$ and all corresponding notations can be found in Fig. 1; square brackets $[\dot{I}]_v$ and $[\ddot{I}]_c$ mean that respective values are taken at retarded times $t - R'/v$ and $t - R'/c$.

In order to bring our numerical evaluations as close as possible to the actual realization of the experiment, we also have taken into consideration the widths of the EA and RA, denoted as h_{EA} and h_{RA}, respectively. Thus, defining the current density per a unit length in the EA as I/h_{EA} we can rewrite Eq. (21) as

$$\varepsilon_p = \frac{1}{4\pi\varepsilon_0 c^2 h_{\mathrm{EA}}}\int_0^{r_{\mathrm{RA}}}\int_0^{2\pi}\int_0^{2\pi}\int_0^{h_{\mathrm{RA}}}\left[\frac{[\dot{I}]_v}{R'^3} + \frac{[\ddot{I}]_c}{R'^2}\right]\Omega(R,r,\theta,\varphi) r_{\mathrm{EA}}^2 r dr d\theta d\varphi dh, \tag{22}$$

where $R' = \sqrt{R'^2_x + R'^2_y + h^2}$.

We used *Mathcad Professional 2000 software* for numerical evaluation of Eq. (22) under the realistic pulsed mode approximation considered in Sec. II C, i.e., for the case of exponential discharge process in the spark gap (SG) when $U(t) = U_0 e^{-t/\tau}$. We took $\tau = 2$ ns as a realistic value for characteristic time of exponential decay estimated for the particular experimental settings described in next section. It allowed us to make a reliable evaluation of $\Delta t(R)$-dependencies (within the approximation $r_{\mathrm{EA}}/R \ll 1$) for different values of the retardation parameter v and plotted in Fig. 6.

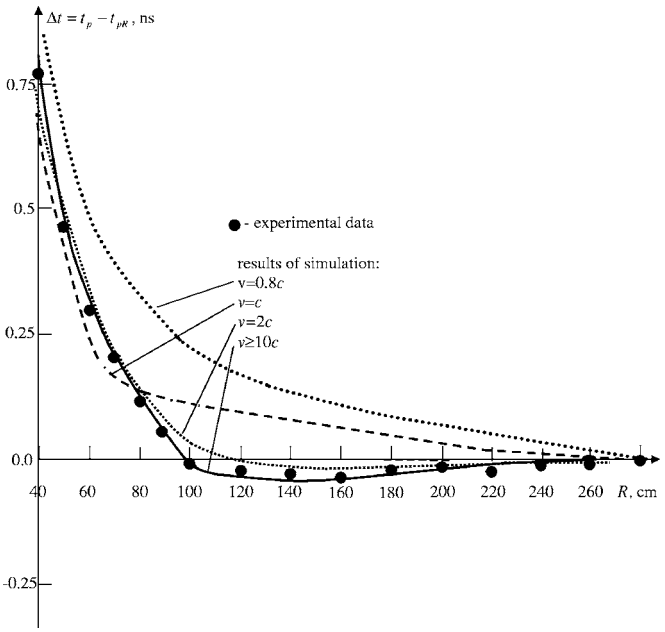

FIG. 6. Comparison of experimental data with the results of numerical calculations of $\Delta t(R)$-dependencies for realistic pulsed mode approximation at the retardation parameters $v=0.8c$, $v=c$, $v=2c$, and $v\geq 10c$ (curves for $v\geq 10c$ are already undistinguishable).

IV. EXPERIMENTAL SETTINGS

The emitting multisection antenna [see Fig. 4(a)] was assembled according to the following geometric parameters: (1) The radius $r=5$ cm; (2) the width $h_{\mathrm{EA}}=5$ cm, and (3) the gap between adjacent sections—0.3 cm. The frame of the EA was made of copper sheet with 1 mm thickness. To deliver a current to every section simultaneously, we used four parallel cables, each one having the characteristic resistance of 50 Ohms and the length of 20 cm. The inductance of the EA (all four sections are connected in parallel) is $L=46\pm 1$ nH. It was measured by the impedance meter *E7–14* (Russia) at frequency 10 kHz.

To charge the *RC* circuit, we used a high-voltage supply of $U\leq 6$ kV. The spark gap *EPCOS A71-H55X 5500V/10A* has 5.5 kV discharge voltage and generates 10 A current flow. Estimated discharge time of the *RC* circuit is 2 ns. The coaxial capacitor *C*, enclosed into the spark gap circuit, has 40 pF, thus determining the proper frequency $\omega_0=1/\sqrt{LC}=7.4\times 10^8\ \mathrm{s}^{-1}$. In this case, according to the definition (18), the critical frequency ω_c is $2.4\times 10^{10}\ \mathrm{s}^{-1}$, hence assuring the validity of the approximation of quasi-stationary current.

The capacitor *C* and the resistor $R_f=5\ \mathrm{M}\Omega$ determine the duration of the period between discharges $T_d\approx 0.3$ ms. A synchronizing time signal was generated by an additional loop antenna with 10 cm diameter and 0.5 cm width (it was placed at 1 m distance below the EA). The spark gap and the capacitor were kept inside the magnetic and electric shielding. It is also worth noting that a relative variation in amplitude of generated signals (caused by the instability of a threshold voltage in SG discharges) did not exceed 5% of the average value.

The geometrical parameters of the RA [see Fig. 4(b)] are: (1) The radius $r=5$ cm; (2) the width $h_{\mathrm{RA}}=10$ cm; and (3) the gap between adjacent sections—0.3 cm. Both sections of this antenna are connected in parallel. Their frames are also made of copper sheet with 1 mm thickness. The inductance of the RA, measured by the impedance meter *E7–14* (Russia) at frequency 10 kHz, is $L=49\pm 1$ nH. The proper rise time of the RA (coupled to the cable of 50 Ω) can be estimated as $\tau_{\mathrm{RA}}=49\ \mathrm{nH}/50\ \Omega\approx 1$ ns. The corresponding critical frequency $\omega_c=1.2\times 10^{10}\ \mathrm{s}^{-1}$ is still one order of magnitude higher than the proper frequency of current oscillations ω_0, keeping the validity of the approximation of the quasi-stationary current for the RA.

To visualize signals generated in the RA, we used 500 MHz digital oscilloscope *Tektronix TDS* 5052 with 5 Gsample/s (0.2 ns per channel) sampling rate. The proper rise time of the oscilloscope is $\tau_o\approx 1$ ns and the expected time resolution is about 0.02 ns. Additionally, the maximal voltage sensitivity available by the oscilloscope is 1 mV/div. Each signal was recorded after 128 averaging. Both EA and RA were mounted on a wooden table and all metallic objects (with the capacity to reflect EM radiation) were removed from the experimental installations at distances exceeding 1.0 m. It assured to make observations in such a manner that during the period of the first 7 ns, all EM perturbations received by the RA could in no way be attributed to reflected fields.

V. EXPERIMENTAL MEASUREMENTS

We remind that zero-crossing method provides the type of variations $\Delta t(R)$ which should be sensitive to the particular value of the retardation parameter v. In Fig. 6 we present the results of numerical calculations for the realistic pulsed mode approximation based on Eq. (22) at the retardation parameters $v=0.8c$, $v=c$, $v=2c$, and $v\geq 10c$ (curves for $v\geq 10c$ are already undistinguishable). It is worth emphasizing that the types of numerical predictions for $v=c$ and $v\geq 10c$ are qualitatively in agreement with the predictions obtained in the case of idealized harmonic signals [see Figs. 2(b) and 3(b)]. The standard condition $v=c$ with respect to bound fields does not imply any negative Δt values for the whole range of variations of *R*. This prediction $\Delta t(R)$ of the standard EM theory can be subjected to the empirical test and should be considered as a reliable verification of the applicability of the standard retardation condition ($v=c$) to the bound fields.

Now we are in a position to apply the zero-crossing method. For this purpose, we placed the EA and RA in parallel positions as it is shown in Fig. 1. Keeping the orientation of antennas unchanged, we varied the distance between them in the range of $R=40-280$ cm, applying the step of $\Delta R=10$ cm (for the range $R=40-100$ cm) and $\Delta R=20$ cm (for the range $R=100-280$ cm). At each position we succeeded in producing detectable signals and stored them in a digital form (see Fig. 7). In order to implement the zero-crossing method, we measured the instant t_{cross} when the oscillating disturbance crosses a zero line for the first time. Even at the maximum distance $R=280$ cm, the amplitude of the whole signal is comparably large (more than 30 mV). It allowed us to measure the value of t_{cross} with due precision. The accuracy in measuring the exact position of a zero-

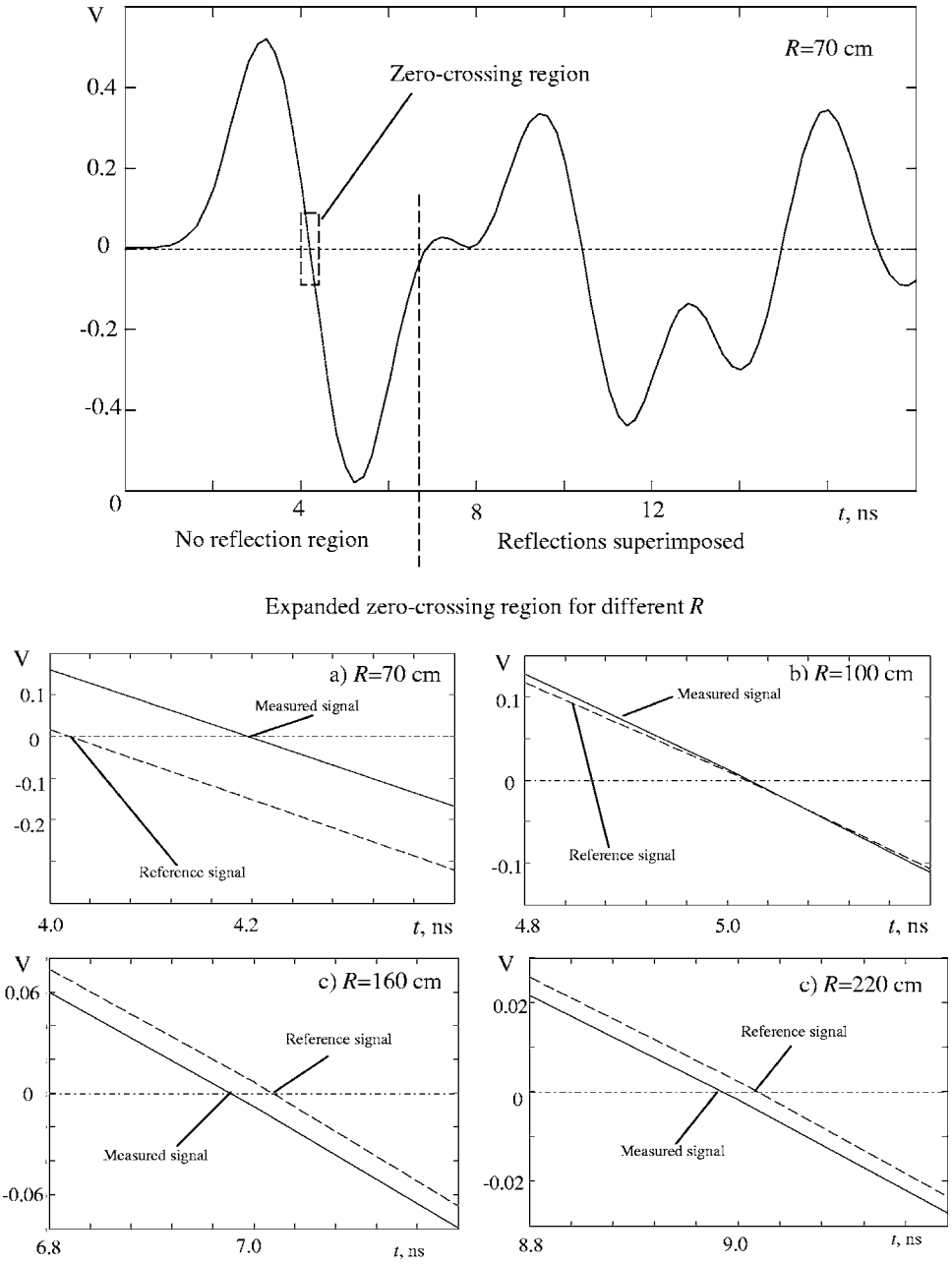

FIG. 7. The detectable signal produced in the RA at the distance $R=70$ cm and stored by the oscilloscope in a digital form. The zero-crossing region is highlighted. Subplots show zero-crossing regions in amplified format and comparison between zero-crossing points of the detected and the reference signals at different distances $R=70$, 100, 160, and 220 cm.

crossing point on the oscilloscope time scale after 128-times averaging was less than the fraction 1/10 of one time channel, i.e., ≤ 0.02 ns.

To complete our measurements we had to obtain the information on the instant t'_{cross} when the reference signal crosses a zero line for the first time. At large distances the radiation R^{-1} predominates and in our case it constitutes more than 99 percent at a distance of 300 cm. It means that at this distance we can take the whole signal as the reference one.

For this purpose, using the digital format available in modern oscilloscopes, we stored the whole signal measured at $R_0=300$ cm (i.e., the reference signal) and recovered its position on oscilloscope time scale at any other smaller distances $R=40\ldots280$ cm in order to make reliable estimations of t'_{cross}. All subplots in Fig. 7 show the radiation R^{-1}-term (dot line) recovered at distances $R=70$, 100, 160, and 220 cm, that are compared with the total signal detected by the oscilloscope.

Figure 7 gives a clear and unambiguous graphic visualization of how the zero-crossing method works in real practice. At $R=70$ cm the front of the reference signal (dot line) goes clearly ahead of the total signal (continuous line) in the region where both oscillations cross a zero line for the first time. It corresponds to a positive value of $\Delta t(R)=t_{\text{cross}}-t'_{\text{cross}}$. Nevertheless, at $R=100$ cm, Δt is already zero and acquires negative values at $R>100$ cm as it can be observed in Fig. 7 at $R=160$ cm and $R=220$ cm. Thus, the resultant experimentally found $\Delta t(R)$-dependence (black circles in Fig. 6) for the range $R=40-280$ cm exhibits a clearly visible negative minimum which should take no place if one expects the validation of the standard retardation condition $v=c$ (the dotted line in Fig. 6) as the conventional EM theory requires.

VI. CONCLUSIONS

Based on these results, one can conclude that experimental data do not support the validity of the standard retardation constraint ($v=c$) generally accepted in respect to bound fields. In our opinion, the circumstance that the presence of this fundamental discrepancy with the predictions of the classical EM theory has not been observed earlier is due to the fact that perhaps there has not been realized the considerable importance in careful drawing and empirical testing distinction between bound and radiation field components. Put in other terms, it has to imply a considerable shift of attention toward the conception of the velocity dependent (bound) components of EM field because they may result of a crucial importance in illuminating possible methodological gaps within empirical verification of some fundamental premises of the classical EM theory.

We also have to point out the fact of a nearly perfect coincidence between experimental data and theoretical predictions based on the Eq. (7) when the retardation parameter v for bound fields highly exceeds the velocity of light, i.e., $v \geq 10c$. Nevertheless, speaking in strict terms, any discrepancy of experimental observations with theoretical predictions made on the basis of the standard condition $v=c$ does not automatically imply the correctness of Eq. (7) with the modified retardation condition in respect to bound components. It implies rather experimentally observed violation of the applicability of the standard retardation condition to bound fields. If this empirical fact is confirmed independently by other methods and approaches, then perhaps it can be characterized as an explicit manifestation of nonlocal properties of bound fields in near zone. At present, nonlocality is generally attributed to the violation of Bell's inequalities in quantum mechanics so that both manifestations of nonlocality might have the same origin. If so, nonlocal characteristics of bound fields promise to shed a new light on a possible close relationship between classical electrodynamics and quantum mechanics.

ACKNOWLEDGMENTS

The authors thank Dr. V. Onoochin (Moscow, Russia) and Dr. I. Moreno (Zacatecas, Mexico) for valuable discussions and J.A. Santamaria-Rueda (Moscow, Russia) for financial support which was a crucial result in the realization of this project.

APPENDIX: DERIVATION OF THE VALUE OF MAGNETIC FIELD DUE TO AN IDEALIZED MAGNETIC DIPOLE UNDER THE GENERAL ASSUMPTION $V>0$

First, it is worth mentioning that Eq. (6) was obtained in Ref. 4 at the low velocity relativistic limit of the exact solution (4) of the D'Alembert Eq. (5) when the centripetal acceleration of moving charges is ignored. The latter requirement implies that in places where the antenna loop is curved, the current I and its time variation $\dot{I}$ are parallel to the tangential direction along the loop. To illustrate the derivation of Eq. (8) from Eq. (7), we follow the standard procedure implemented in Ref. 5

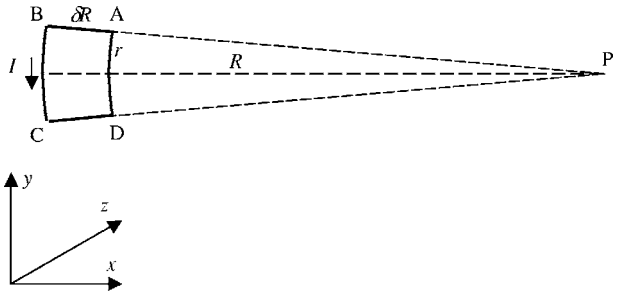

FIG. 8. Sections AD and BC are arcs of circles with the radii R and $R+\delta R$, respectively, with the common center at the point of observation P. The length of the section AD is equal to r, and for $r \ll R$, the length of the section BC is $r(1+\delta R/R)$. Conduction current I flows in the counter clockwise direction.

Thus, if the radius r of the loop of the antenna is negligible in comparison with the distance to the point of observation R, i.e., $r \ll R$, then the shape of the antenna has no importance and it can be chosen in a way to simplify theoretical calculations. So, let us consider the small current carrying coil $ABCD$ shown in Fig. 8. An arrow indicates the direction of the conduction current. Sections AD and BC are arcs circles, with centers at the point of observation P. Both circles have the radius value R and $R+\delta R$, respectively, where $\delta R \ll R$. Thus, if the length of the section AD is equal to r (where $r \ll R$), then the length of BC is $r(1+\delta R/R)$.

Let us now determine the magnetic field $\mathbf{B}$ at the point of observation P and at the time of observation t. According to Eq. (7) the contributions of the currents in the sections AB and CD are both zero since $\mathbf{k} \times \mathbf{n} = 0$. Thus, we can calculate the value of the magnetic field generated only by the sections BC and AD:

$$\mathbf{B} = \frac{1}{4\pi\varepsilon_0 c^2} \oint_{BC+AD} \left\{ \frac{[I]_v}{R^2} + \frac{[\dot{I}]_c}{cR} \right\} \mathbf{k} \times \mathbf{n} dl. \tag{A1}$$

Integrating Eq. (A1) we obtain the value of the magnetic field generated by the section BC:

$$\mathbf{B}_{BC} = \frac{1}{4\pi\varepsilon_0 c^2} \left\{ [I]_v \frac{r(1+\delta R/R)}{R^2(1+\delta R/R)^2} + [\dot{I}]_c \frac{r(1+\delta R/R)}{cR(1+\delta R/R)} \right\} \mathbf{k}, \tag{A2}$$

and by the section AD, respectively,

$$\mathbf{B}_{AD} = -\frac{1}{4\pi\varepsilon_0 c^2} \left\{ [I]_v \frac{r}{R^2} + [\dot{I}]_c \frac{r}{cR} \right\} \mathbf{k}. \tag{A3}$$

Since $\delta R/R \ll 1$, the use of the binomial theorem is justified and Eq. (A2) takes a more compact form

$$\mathbf{B}_{BC} = \frac{1}{4\pi\varepsilon_0 c^2} \left\{ [I]_v \frac{r}{R^2} \left(1 - \frac{\delta R}{R} \right) + [\dot{I}]_c \frac{r}{cR} \right\} \mathbf{k}. \tag{A4}$$

The circumstance that the section AD is placed closer to the point of observation P means that any signal traveling with the finite velocity and produced in this section at some initial instant t_0 will arrive at the point P earlier than its BC counterpart, generated at the same time t_0.

Under the retardation rate v, bound components of the magnetic fields $\mathbf{B}_{BC}$ and $\mathbf{B}_{AD}$ arrive at the point of observation P with different values of retardation time $t'=t-(R+\delta R)/v$ and $t'=t-R/v$, respectively. Therefore, both values of current $[I]_v$ in (A2) and (A3) have been generated at different initial instants of time $t_0^{BC}=t-(R+\delta R)/v$ and $t_0^{AD}=t-R/v$, where t is the time of observation at P. The shift between t_0^{BC} and t_0^{AD} is $\Delta t_v=t_0^{AD}-t_0^{BC}=\delta R/v$. Both values $I(t_0^{BC})$ and $I(t_0^{AD})$ can be related if one knows the rate of change of current $\dot{I}$ in one of the sections

$$I(t_0^{BC})=I\left(t_0^{AD}-\frac{\delta R}{v}\right)=I(t_0^{AD})-\dot{I}(t_0^{AD})\delta R/v$$

$$=[I]_v-[\dot{I}]_v\frac{\delta R}{v}, \tag{A5}$$

where $I(t_0^{AD})=[I]_\nu$ and $\dot{I}(t_0^{AD})=[\dot{I}]_\nu$ are evaluated at the retarded time $t'=t-R/v$.

The same reasoning is also applicable to the radiation components which will arrive at P with different values of retardation time $t'=t-(R+\delta R)/c$ and $t'=t-R/c$, respectively. The shift between corresponding values of retardation time is $\Delta t_{v=c}=t_0^{AD}-t_0^{BC}=\delta R/c$. By analogy with (A5), it determines the following relationship:

$$\dot{I}(t_0^{BC})=\dot{I}\left(t_0^{AD}-\frac{\delta R}{c}\right)=\dot{I}(t_0^{AD})-\ddot{I}(t_0^{AD})\frac{\delta R}{c}=[I]_c-[\ddot{I}]_c\frac{\delta R}{c}, \tag{A6}$$

where $\dot{I}(t_0^{AD})=[\dot{I}]_c$ and $\ddot{I}(t_0^{AD})=[\ddot{I}]_c$ are evaluated at the retarded time $t'=t-R/c$.

Thus, neglecting all terms proportional to $(\delta R)^2$, Eq. (A6) can be rewritten as follows:

$$\mathbf{B}_{BC}=\frac{1}{4\pi\varepsilon_0 c^2}\left\{[I]_v\left(1-\frac{\delta R}{R}\right)\frac{r}{R^2}-[\dot{I}]_v\frac{r}{R^2}\frac{\delta R}{v}+[\dot{I}]_c\frac{r}{cR}-[\ddot{I}]_c\frac{r\delta R}{c^2R}\right\}\mathbf{k}. \tag{A7}$$

Adding Eqs. (A7) and (A8) we find the resultant magnetic field at the point P and the time t

$$\mathbf{B}=\frac{\Delta S}{4\pi\varepsilon_0 c^2}\left\{\frac{[I]_v}{R^3}+\frac{c}{v}\frac{[\dot{I}]_v}{cR^2}+\frac{[\ddot{I}]_c}{c^2R}\right\}\mathbf{k}, \tag{A8}$$

where we have taken into account that the area of the loop $ABCD$ is $\Delta S=r\delta R$.

[1] J. D. Jackson, *Classical Electrodynamics*, 2nd ed. (Wiley, New York, 1975).
[2] L. D. Landau and E. M. Lifshitz, *The Classical Theory of Fields* (Addison-Wesley, Cambridge, MA, 1951).
[3] H. Hertz, in *Electric Waves, Collection of Scientific Papers* (Dover, New York, 1962), p. 108.
[4] O. D. Jefimenko, *Electricity and Magnetism: An Introduction to the Theory of Electric and Magnetic Fields*, 2nd ed. (Electret Scientific Co., Star City, WV, 1989).
[5] W. G. V. Rosser, *Interpretation of Classical Electromagnetism, Fundamental Theories of Physics*, edited by A. Van der Merwe (Kluwer Academic, Dordrecht, 1997), Vol. 78.
[6] J. A. Stratton, *Electromagnetic Theory* (McGraw-Hill, New York, 1941).
[7] H. Knöpfel, *Pulsed High Magnetic Fields* (North-Holland, Amsterdam, 1970).